Liquid Crystals
Publication details, including instructions for authors and subscription information:
http://www.informaworld.com/smpp/title~content=t713926090

Synthesis and characterization of achiral banana-shaped liquid crystalline molecules containing bisnaphthyl moieties

Po-Jen Yang[a]; Hong-Cheu Lin[a]
[a] Department of Materials Science and Engineering, National Chiao Tung University, Taiwan, ROC

To cite this Article Yang, Po-Jen and Lin, Hong-Cheu(2006) 'Synthesis and characterization of achiral banana-shaped liquid crystalline molecules containing bisnaphthyl moieties', Liquid Crystals, 33: 5, 587 — 603
To link to this Article: DOI: 10.1080/02678290600633394
URL: http://dx.doi.org/10.1080/02678290600633394

Liquid Crystals, Vol. 33, No. 5, May 2006, 587–603

Synthesis and characterization of achiral banana-shaped liquid crystalline molecules containing bisnaphthyl moieties

PO-JEN YANG and HONG-CHEU LIN*

Department of Materials Science and Engineering, National Chiao Tung University, Hsinchu, Taiwan, ROC

(*Received 29 September 2005; accepted 6 January 2006*)

Three analogous series of symmetric banana-shaped liquid crystalline molecules containing bisnaphthyl units were synthesized and characterized. The effects of linking groups (on the side wings) and lateral *meta*-fluoro substitutions (on the middle outer rings) on the mesogenic properties were examined. The type of mesophase depends on the lengths of terminal alkoxy chains. Thus, achiral molecules with shorter flexible chains (n=8) exhibit a rectangular columnar (B_1) phase, while analogous derivatives with longer flexible chains (n=12) display the B_2 phase. All lateral *meta*-fluoro substituted analogues (series **II**) possess the lowest isotropization temperatures and the narrowest mesophasic ranges of the B_1 and B_2 phases. The B_1 and B_2 phases were confirmed by X-ray diffraction, polarizing optical microscopy (POM) and electro-optical (EO) switching experiments. An electric field-induced transition from an antiferroelectric (tristable) state to a ferroelectric (bistable) state was observed in the EO measurements. Spontaneous polarization (by switching current response), tilt angle of chiral domains (by POM), and transmittance–voltage measurements of the B_2 phase in related compounds have been surveyed in this study.

1. Introduction

Since the first ferroelectric liquid crystalline (FLC) material was reported by Meyer *et al*. in 1975 [1], FLCs were characterized as tilted arrangements of smectic liquid crystalline phases in materials composed of chiral molecules, allowing the occurrence of spontaneous polarizations. Later, antiferroelectric liquid crystals (AFLCs) were discovered and finally identified in 1989 [2]; subsequently, AFLCs were developed into fast electro-optic devices due to the quick response of these materials used for flat-panel displays [3].

In 1996, Niori *et al*. [4] first demonstrated that smectic phases of achiral molecules with bent cores can exhibit ferroelectric switching properties. These achiral molecules have a sterically induced polar packing character, and are arranged in smectic layers in such a way that the dipoles point along a common direction within the layer, and tilt with respect to the layer normal. These factors can give rise to chiral layer symmetry, although the molecules themselves are achiral. These liquid crystalline molecules with a bent molecular shape, so-called banana-shaped liquid crystals, have attracted much attention owing to their novel ferroelectric properties. Although eight different banana phases (B_1 to B_8) of achiral molecules have been identified [5, 6] electro-optical switching behaviour is observed only in the smectic B_2, B_5 and B_7 phases. Among these phases with switching properties, the B_2 phase is the most frequently investigated. According to the report of Link *et al*. [7], the spontaneous formation of macroscopic chiral domains in a fluid smectic is derived from achiral molecules with antiferroelectric switching characteristics. The B_2 phase exhibit four different supramolecular architectures, denoted SmC_AP_A, SmC_SP_A, SmC_AP_F and SmC_SP_F; here synclinic (S) or anticlinic (A) represents molecular tilt correlation, and ferroelectric (F) or antiferroelectric (A) specifies polar correlation between adjacent layers. When the layer chiralities in adjacent layers have the same handedness, such as those in SmC_AP_A and SmC_SP_F, the structures are called homochiral; whereas, when the chiralities in adjacent layers alternate, such as those in SmC_AP_F and SmC_SP_A, the structures are called racemic. More recently, different parts of the achiral molecular structures, such as the central parts, lateral substituents, linking groups, terminal chains, and the number of rings, have been varied to study the influence of molecular design on the mesomorphic behaviour [5, 8–14].

In this study, three analogous series of symmetric banana-shaped liquid crystalline molecules containing bisnaphthyl units were synthesized and characterized. All these compounds are derived from central resorcinol

*Corresponding author. Email: linhc@cc.nctu.edu.tw

Liquid Crystals
ISSN 0267-8292 print/ISSN 1366-5855 online © 2006 Taylor & Francis
http://www.tandf.co.uk/journals
DOI: 10.1080/02678290600633394

cores and connected by ester linking groups, and the side wings of the molecules are connected via ester or Schiff base linkages symmetrically, with different lengths (n=8, 12 and 16) of flexible alkoxy chains. Their molecular structures are shown in figure 1, which includes three variable parts; i.e. with/without lateral substitutions (X=F or H), different linking groups (Y=–COO– or –CH=N–), and alkoxy flexible tails with three different lengths of n.

2. Experimental

2.1. *Characterization*

^{1}H NMR spectra were recorded on a Varian unity 300 MHz spectrometer using $CDCl_3$ and DMSO-d_6 as solvents. Elemental analyses were performed on a Heraeus CHN-OS RAPID elemental analyser. Mesophase textures were characterized by a polarizing optical microscopy (POM) using a Leica DMLP equipped with a hot stage. Temperatures and enthalpies of transition were determined by differential scanning calorimetry (DSC) using a Perkin-Elmer Pyris 7, under N_2 at a heating and cooling rate of 5°C min^{-1}.

Synchrotron powder X-ray diffraction (XRD) measurements were performed at beamline BL17A of the National Synchrotron Radiation Research Center (NSRRC), Taiwan, where the X-ray wavelength was 1.32633 Å. The XRD data were collected using imaging plates (IP, of an area=20 × 40 cm^2 and a pixel resolution of 100) curved with a radius equivalent to a sample-to-image plate distance of 280 mm, and the diffraction signals were accumulated for 3 min. The powder samples were packed into a capillary tube and heated by a heat gun, whose temperature controller is programmable by a PC with a PID feedback system. The scattering angle theta was calibrated by a mixture of silver behenate and silicon.

The electro-optical properties were determined in commercially available ITO cells (from Mesostate Corp., thickness=9 μm, active area=0.25 cm^2) with rubbed polyimide alignment coatings (antiparallel rubbing direction). The optical transmission experiments used cells of active area=1 cm^2, 6 μm thick (antiparallel rubbing direction), with monochromatic light from a He-Ne laser beam (632.8 nm). The cell was placed between crossed polarizers and its orientation was adjusted to obtain the minimum transmission of light (detected by a photodiode) without an electric field. The photodiode detector was set about 20 cm away from the cell sample, with the incident laser beam normal to the cell. A digital oscilloscope (Tektronix TDS-3012B) was used in these measurements, and a high power amplifier connected to a function generator (GW Model GFG-813) with a d.c. power supply (Keithley 2400) was utilized in the d.c. field experiments. During electro-optical measurements, texture modulations on applying an electric field were observed by POM.

2.2. *Synthesis*

Chemicals and solvents were reagent grades and purchased from Aldrich, ACROS, TCI and Lancaster Chemical Co. Dichloromethane (CH_2Cl_2) was redistilled under nitrogen and dried over calcium hydride before use. The other chemicals were used without further purification.

The synthetic route to the banana-shaped compounds of this study is shown in scheme 1 (series **I** and **II**) and scheme 2 (series **III**). 6-*n*-Alkoxynaphthalene-2-carboxylic acids were prepared according to literature procedures. 6-Hydroxynaphthalene-2-carboxylic acid was converted to methyl 6-hydroxynaphthalene-2-carboxylate using the modified procedure described by Güller *et al.* [15]; this ester was treated with the appropriate *n*-alkyl bromides followed by hydrolysis [16]. 6-*n*-Alkoxynaphthalene-2-carbaldehyde [17] and 4-benzyloxybenzoic acid [18] were synthesized according to the respective literature procedures.

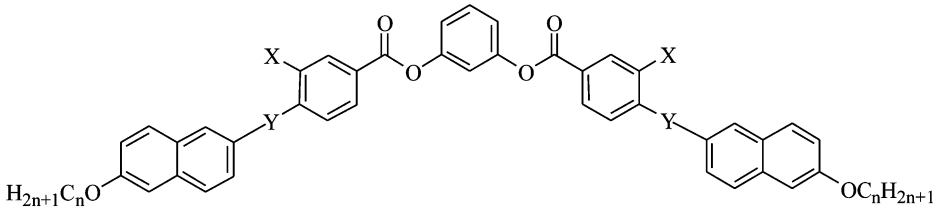

Series **I** (**a-c**): X = H and Y = -COO-
Series **II** (**a-c**): X = F and Y = -COO-
Series **III** (**a-c**): X = H and Y = -CH=N-
where n = 8, 12, and 16 for a, b, and c, respectively.

Figure 1. Molecular structures of the synthesized series I, II and III compounds.

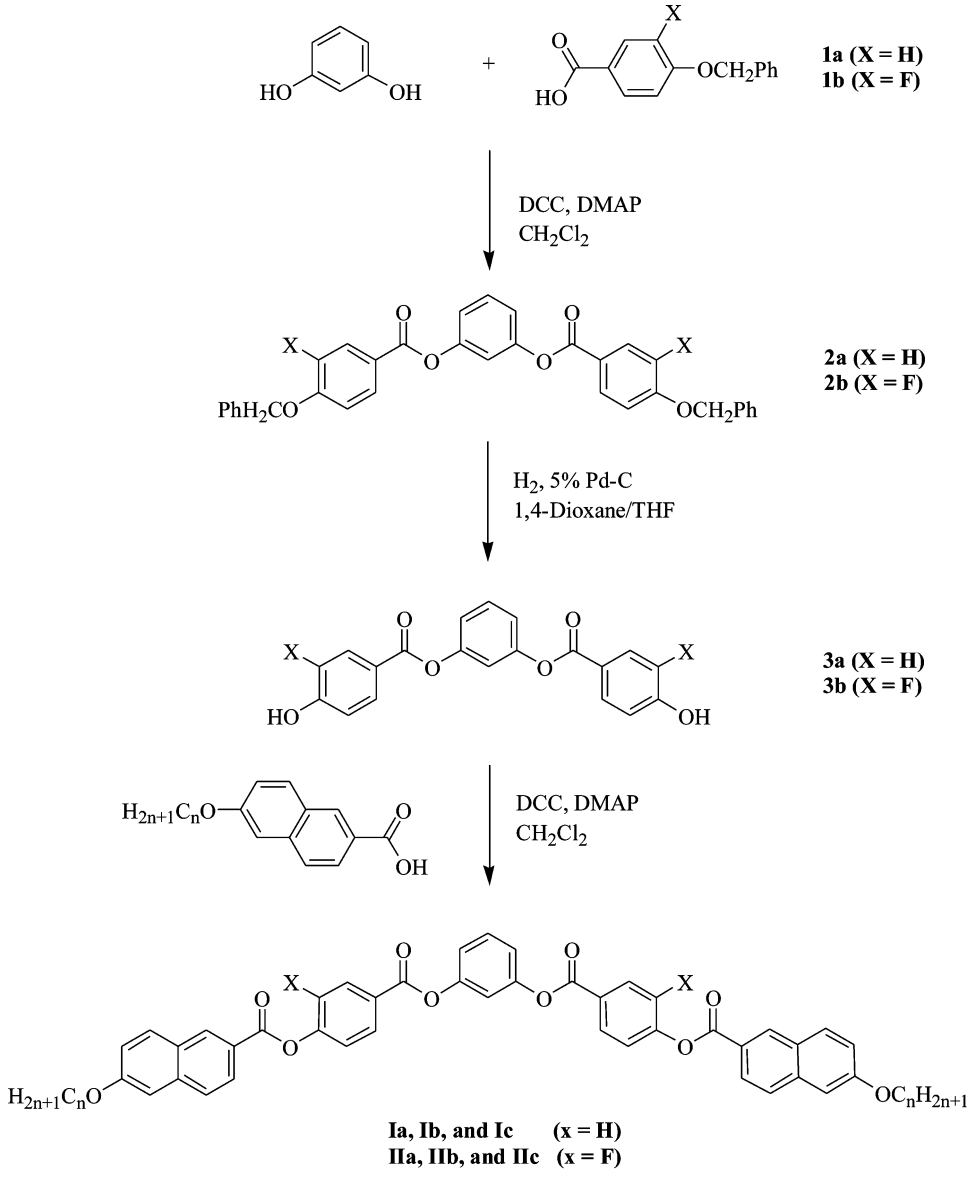

Scheme 1. Synthetic route for series **I** and **II** compounds.

3-Fluoro-4-benzyloxybenzoic acid was prepared as described in [19], followed by a similar procedure to that for 4-benzyloxybenzoic acid.

2.2.1. 1,3-Phenylene bis(4-benzyloxybenzoate), 2a (*X*=H). To a suspension of resorcinol (1.5 g, 13.6 mmol) in a solution of 4-benzyloxybenzoic acid **1a** (6.2 g, 27.2 mmol) in dry dichloromethane (60 ml), were added *N*,*N*-dicyclohexylcarbodiimide (DCC) (5.9 g, 28.6 mmol) and a catalytic amount of 4-(*N*,*N*-dimethylamino)pyridine (DMAP). The reaction mixture was stirred under nitrogen for 15 h at room temperature. The precipitated dicyclohexylurea (DCU) was filtered off and washed with an excess of $CHCl_3$ (100 ml). The filtrate was washed with water and dried over anhydrous magnesium sulphate. After removal of the solvent by evaporation under reduced pressure, the residue was purified by column chromatography (silica gel, $CHCl_3$). The collected product was crystallized from a mixture of dichloromethane and 2-propanol to give a white solid; yield 5.1 g (71%). ^{1}H NMR (ppm, $CDCl_3$): 8.16 (d, J=8.9 Hz, 4H, Ar–H), 7.49−7.35 (m, 10H, Ar–H), 7.16−7.13 (m, 4H, Ar–H), 7.07 (d, J=8.9 Hz, 4H, Ar–H), 5.16 (s, 4H, $ArCH_2O$–).

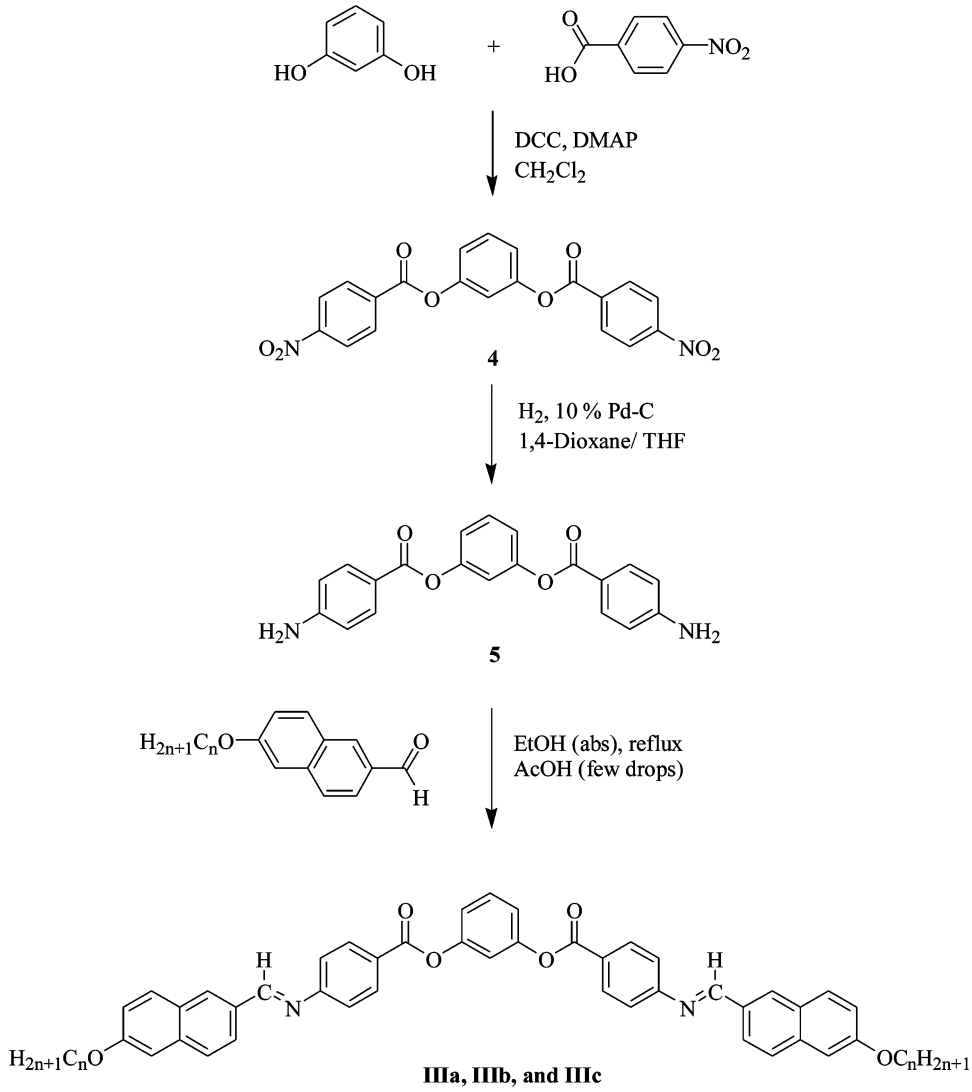

Scheme 2. Synthetic route for series **III** compounds.

2.2.2. 1,3-Phenylene bis(3-fluoro-4-benzyloxybenzoate), 2b (*X*=F). This compound was obtained from the reaction of resorcinol and 3-fluoro-4-benzyloxybenzoic acid **1b**, following a similar procedure to that described for compound **2a**. The product was isolated as a white solid; yield 69%. ^{1}H NMR (ppm, $CDCl_3$): 7.94−7.88 (m, 4H, Ar–H), 7.47−7.35 (m, 11H, Ar–H), 7.14−7.06 (m, 5H, Ar–H), 5.25 (s, 4H, $ArCH_2O$–).

2.2.3. 1,3-Phenylene bis(4-hydroxybenzoate), 3a (*X*=H). Compound **2a** (5 g, 9.4 mmol), was dissolved in a mixture of 1,4-dioxane (200 ml) and THF (100 ml) containing a suspension of 10% Pd-C catalyst (1 g). The mixture was stirred under hydrogen at room temperature until no further hydrogen was taken up (*c*. 10 h). The catalyst was removed by filtration through Celite and washed with THF (100 ml). The solvent was removed by evaporation under reduced pressure and the crude product purified by column chromatography (silica gel, $CHCl_3$/EtOAc 60/1) to give a white solid; yield 90%. ^{1}H NMR (ppm, DMSO-d_6): 10.54 (s, 2H, 2 × Ar–OH), 7.98 (d, *J*=8.7 Hz, 4H, Ar–H), 7.49 (t, *J*=8.7 Hz, 1H, Ar–H), 7.20−7.17 (m, 3H, Ar–H), 6.92 (d, *J*=8.7 Hz, 4H, Ar–H).

2.2.4. 1,3-Phenylene bis(3-fluoro-4-hydroxybenzoate), 3b (*X*=F). This compound was obtained from

compound **2b**, following a similar procedure to that described for compound **3a**. The product was isolated as a white solid; yield 92%. ^{1}H NMR (ppm, DMSO-d_6): 11.09 (br s, 2H, 2 × Ar–OH), 7.86−7.80 (m, 4H, Ar–H), 7.52 (t, J=8.4 Hz, 1H, Ar–H), 7.27−7.15 (m, 3H, Ar–H), 7.12−7.09 (m, 2H, Ar–H).

Compounds of series **I** and series **II** were prepared by similar methods to that described for compound **2a**. After work-up, the crude products were purified by column chromatography (silica gel, $CHCl_3$) and twice recrystallized from a mixture of chloroform and ethanol. The yields of these products after purification were *c*. 50–65%.

2.2.5. 1,3-Phenylene bis[4-(6-*n*-octyloxynaphthalene-2-carbonyloxy)benzoate], Ia (*n*=8). The crude product was isolated as a white solid from the reaction of compound **3a** with 6-*n*-octyloxynaphalene-2-carboxylic acid. ^{1}H NMR (ppm, $CDCl_3$): 8.72 (s, 2H, Ar–H), 8.31 (d, J=8.7 Hz, 4H, Ar–H), 8.15 (d, J=8.7 Hz, 2H, Ar–H), 7.90 (d, J=9.0 Hz, 2H, Ar–H), 7.82 (d, J=9.0 Hz, 2H, Ar–H), 7.51 (t, J=8.4 Hz, 1H, Ar–H), 7.44 (d, J=8.7 Hz, 4H, Ar–H), 7.26−7.19 (m, 7H, Ar–H), 4.12 (t, J=6.6 Hz, 4H, 2 × OCH_2), 1.93−1.86 (m, 4H, 2 × $OCH_2\underline{CH_2}$), 1.55−1.31 (m, 20H, 10 × CH_2), 0.90 (t, J=6.6 Hz, 6H, 2 × CH_3). Anal: calc. for $C_{58}H_{58}O_{10}$, C 76.13, H 6.39; found, C 76.04, H 6.60%.

2.2.6. 1,3-Phenylene bis[4-(6-*n*-dodecyloxynaphthalene-2-carbonyloxy)benzoate], Ib (*n*=12). The crude product was isolated as a white solid from the reaction of compound **3a** with 6-*n*-dodecyloxynaphalene-2-carboxylic acid. ^{1}H NMR (ppm, $CDCl_3$): 8.72 (s, 2H, Ar–H), 8.31 (d, J=8.7 Hz, 4H, Ar–H), 8.15 (d, J=8.7 Hz, 2H, Ar–H), 7.90 (d, J=9.0 Hz, 2H, Ar–H), 7.82 (d, J=9.0 Hz, 2H, Ar–H), 7.53 (t, J=8.4 Hz, 1H, Ar–H), 7.44 (d, J=8.7 Hz, 4H, Ar–H), 7.26−7.19 (m, 7H, Ar–H), 4.12 (t, J=6.6 Hz, 4H, 2 × OCH_2), 1.90−1.83 (m, 4H, 2 × $OCH_2\underline{CH_2}$), 1.56−1.28 (m, 36H, 18 × CH_2), 0.90 (t, J=6.6 Hz, 6H, 2 × CH_3). Anal: calc. for $C_{66}H_{74}O_{10}$, C 77.16, H 7.26; found C 77.07, H 7.28%.

2.2.7. 1,3-Phenylene bis[4-(6-*n*-hexadecyloxynaphthalene-2-carbonyloxy)benzoate], Ic (*n*=16). The crude product was isolated as a white solid from the reaction of compound **3a** with 6-*n*-hexadecyloxynaphalene-2-carboxylic acid. ^{1}H NMR (ppm, $CDCl_3$): 8.72 (s, 2H, Ar–H), 8.31 (d, J=8.7 Hz, 4H, Ar–H), 8.15 (d, J=8.7 Hz, 2H, Ar–H), 7.90 (d, J=9.0 Hz, 2H, Ar–H), 7.82 (d, J=9.0 Hz, 2H, Ar–H), 7.53 (t, J=8.4 Hz, 1H, Ar–H), 7.44 (d, J=8.7 Hz, 4H, Ar–H), 7.26−7.19 (m, 7H, Ar–H), 4.12 (t, J=6.6 Hz, 4H, 2 × OCH_2), 1.90−1.82 (m, 4H, 2 × $OCH_2\underline{CH_2}$), 1.55−1.31 (m, 52H, 26 × CH_2), 0.90 (t, J=6.6 Hz, 6H, 2 × CH_3). Anal: calc. for $C_{74}H_{90}O_{10}$, C 78.00, H 7.96; found, C 78.23, H 7.97%.

2.2.8. 1,3-Phenylene bis[4-(6-*n*-octyloxynaphthalene-2-carbonyloxy)-3-fluorobenzoate], IIa (*n*=8). The crude product was isolated as a white solid from the reaction of compound **3b** with 6-*n*-octyloxynaphalene-2-carboxylic acid. ^{1}H NMR (ppm, $CDCl_3$): 8.73 (s, 2H, Ar–H), 8.17−8.06 (m, 6H, Ar–H), 7.90 (d, J=9.0 Hz, 2H, Ar–H), 7.82 (d, J=8.7 Hz, 2H, Ar–H), 7.51−7.47 (m, 3H, Ar–H), 7.26−7.19 (m, 7H, Ar–H), 4.12 (t, J=6.6 Hz, 4H, 2 × OCH_2), 1.92−1.83 (m, 4H, 2 × $OCH_2\underline{CH_2}$), 1.54−1.31 (m, 20H, 10 × CH_2), 0.90 (t, J=6.6 Hz, 6H, 2 × CH_3). Anal: calc. for $C_{58}H_{56}F_2O_{10}$, C 73.25, H 5.93; found, C 73.28, H 6.06%.

2.2.9. 1,3-Phenylene bis[4-(6-*n*-dodecyloxynaphthalene-2-carbonyloxy)-3-fluorobenzoate], IIb (*n*=12). The crude product was isolated as a white solid from the reaction of compound **3b** with 6-*n*-dodecyloxynaphalene-2-carboxylic acid. ^{1}H NMR (ppm, $CDCl_3$): 8.73 (s, 2H, Ar–H), 8.17−8.06 (m, 6H, Ar–H), 7.90 (d, J=9.0 Hz, 2H, Ar–H), 7.82 (d, J=8.7 Hz, 2H, Ar–H), 7.55−7.49 (m, 3H, Ar–H), 7.26−7.19 (m, 7H, Ar–H), 4.12 (t, J=6.6 Hz, 4H, 2 × OCH_2), 1.90−1.85 (m, 4H, 2 × $OCH_2\underline{CH_2}$), 1.54−1.28 (m, 36H, 18 × CH_2), 0.88 (t, J=6.6 Hz, 6H, 2 × CH_3). Anal: calc. for $C_{66}H_{72}F_2O_{10}$, C 74.55, H 6.83; found, C 74.45, H 6.94%.

2.2.10. 1,3-Phenylene bis[4-(6-*n*-hexadecyloxynaphthalene-2-carbonyloxy)-3-fluorobenzoate], IIc (*n*=16). The crude product was isolated as a white solid from the reaction of compound **3b** with 6-*n*-hexadecyloxynaphalene-2-carboxylic acid. ^{1}H NMR (ppm, $CDCl_3$): 8.73 (s, 2H, Ar–H), 8.17−8.06 (m, 6H, Ar–H), 7.90 (d, J=9.0 Hz, 2H, Ar–H), 7.82 (d, J=8.7 Hz, 2H, Ar–H), 7.55−7.49 (m, 3H, Ar–H), 7.26−7.19 (m, 7H, Ar–H), 4.12 (t, J=6.6 Hz, 4H, 2 × OCH_2), 1.88−1.83 (m, 4H, 2 × $OCH_2\underline{CH_2}$), 1.54−1.28 (m, 52H, 26 × CH_2), 0.90 (t, J=6.6 Hz, 6H, 2 × CH_3). Anal: calc. for $C_{74}H_{88}F_2O_{10}$, C 75.61, H 7.55; found C 75.20, H 7.53%.

2.2.11. 3-(4-Nitrobenoyloxy)phenyl 4-nitrobenzoate, 4. This compound was obtained from resorcinol and 4-nitrobenzoic acid, following a similar procedure to that described for compound **2a**. After work up, the crude product was purified by column chromatography (silica gel, $CHCl_3$/EtOAc 20/1), and recrystallized from a mixture of dichloromethane and ethanol. The product

was isolated as a yellow solid; yield 80%. ^{1}H NMR (ppm, $CDCl_3$): 8.38 (s, 8H, Ar–H), 7.54 (t, J=8.1 Hz, 1H, Ar–H), 7.25−7.22 (m, 3H, Ar–H).

2.2.12. 3-(4-Aminobenzoyloxy)phenyl 4-aminobenzoate, 5. This compound was obtained from compound **4**, following a similar procedure to that described for compound **3a**. After work-up, the crude product was purified by column chromatography (silica gel, $CHCl_3$/EtOAc 2/1). The product was isolated as a white solid; yield 89%. ^{1}H NMR (ppm, $CDCl_3$): 7.78 (d, J=8.7 Hz, 4H, Ar–H), 7.45 (t, J=7.8 Hz, 1H, Ar–H), 7.12−7.08 (m, 3H, Ar–H), 6.62 (d, J=8.7 Hz, 4H, Ar–H), 4.16 (s, 4H, Ar–NH_2).

2.2.13. 1,3-Phenylene bis[4-(6-*n*-octyloxynaphthalen-2-ylideneamino)benzoate], IIIa (*n*=8). A few drops of acetic acid (glacial) were added to a solution of compound **5** (0.4 g, 1.15 mmol) and 6-*n*-octyloxynaphthalene-2-carbaldehyde (0.69 g, 2.42 mmol) dissolved in absolute ethanol (50 ml). The mixture was heated at reflux for 4 h, then cooled to room temperature. The precipitated product was filtered off and, washed with hot absolute ethanol. It was purified by several recrystallizations from a chloroform and ethanol mixture to give a yellow solid; yield 0.35 g (35%). ^{1}H NMR (ppm, $CDCl_3$): 8.57 (s, 2H, –CH=N–), 8.25 (d, J=8.4 Hz, 4H, Ar–H), 8.16 (s, 2H, Ar–H), 8.12 (d, J=8.7 Hz, 2H, Ar–H), 7.82 (t, J=9.6 Hz, 4H, Ar–H), 7.48 (t, J=8.4 Hz, 1H, Ar–H), 7.27 (d, J=8.4 Hz, 4H, Ar–H), 7.24−7.18 (m, 7H, Ar–H), 4.01 (t, J=6.6 Hz, 4H, $2\times OCH_2$), 1.92−1.82 (m, 4H, $2\times OCH_2\underline{CH_2}$), 1.57−1.26 (m, 20H, $10\times CH_2$), 0.90 (t, J=6.6 Hz, 6H, $2\times CH_3$). Anal: calc. for $C_{58}H_{60}N_2O_6$, C 79.06, H 6.86, N 3.18; found, C 79.06, H 7.03, N 3.43%.

2.2.14. 1,3-Phenylene bis[4-(6-*n*-dodecyloxynaphthalen-2-ylideneamino)benzoate], IIIb (*n*=12). The crude product was isolated as a yellow solid from the reaction of compound **6** with 6-*n*-dodecyloxynaphthalene-2-carbaldehyde, following a similar procedure to that described for compound **IIIa**; yield 40%. ^{1}H NMR (ppm, $CDCl_3$): 8.57 (s, 2H, −CH=N−), 8.25 (d, J=8.4 Hz, 4H, Ar–H), 8.17 (s, 2H, Ar–H), 8.12 (d, J=8.4 Hz, 2H, Ar–H), 7.85 (t, J=9.3 Hz, 4H, Ar–H), 7.52 (t, J=8.4 Hz, 1H, Ar–H), 7.32 (d, J=8.7 Hz, 4H, Ar–H), 7.26−7.18 (m, 7H, Ar–H), 4.11 (t, J=6.6 Hz, 4H, $2\times OCH_2$), 1.92−1.83 (m, 4H, $2\times OCH_2\underline{CH_2}$), 1.58−1.28 (m, 36H, $18\times CH_2$), 0.88 (t, J=6.6 Hz, 6H, $2\times CH_3$). Anal: calc. for $C_{66}H_{76}N_2O_6$, C 79.80, H 7.71, N 2.82; found, C 79.46, H 7.64, N 2.81%.

2.2.15. 1,3-Phenylene bis[4-(6-*n*-hexadecyloxynaphtha1len-2-ylideneamino)-benzoate], IIIc (*n*=16). The crude product was isolated as a yellow solid from the reaction of compound **6** with 6-*n*-hexadecyloxynaphthalene-2-carbaldehyde, following a similar procedure to that described for compound **IIIa**; yield 42%. ^{1}H NMR (ppm, $CDCl_3$): 8.57 (s, 2H, −CH=N−), 8.25 (d, J=8.4 Hz, 4H, Ar–H), 8.17 (s, 2H, Ar–H), 8.12 (d, J=8.4 Hz, 2H, Ar–H), 7.85 (t, J=9.3 Hz, 4H, Ar–H), 7.52 (t, J=8.4 Hz, 1H, Ar–H), 7.32 (d, J=8.7 Hz, 4H, Ar–H), 7.26−7.18 (m, 7H, Ar–H), 4.11 (t, J=6.6 Hz, 4H, $2\times OCH_2$), 1.90−1.82 (m, 4H, $2\times OCH_2\underline{CH_2}$), 1.54−1.28 (m, 52H, $26\times CH_2$), 0.90 (t, J=6.6 Hz, 6H, $2\times CH_3$). Anal: calc. for $C_{74}H_{92}N_2O_6$, C 80.39, H 8.39, N 2.53; found, C 79.87, H 8.35, N 2.46%.

3. Results and discussion

3.1. *Mesophases and thermal properties*

The phase transition temperatures and corresponding enthalpy changes of all the compounds obtained from differential scanning calorimetry (DSC) are summarized in table 1. Only one mesophase (either B_1 or B_2) was observed for each compound in both series; then exhibited monotropic or enantiotropic phase behaviour. The mesomorphic behaviour is significantly influenced by the terminal alkoxy flexible chains. All compounds bearing the longest chain length (n=16) in the three analogous series show the B_2 phase (**Ic** and **IIIc** are enantiotropic but **IIc** is monotropic). In contrast, the analogous compounds bearing the shortest chain length (n=8) show the B_1 phase (**Ia** and **IIa** are enantiotropic but **IIIa** is monotropic).

The B_1 phase exhibits both mosaic-like and dendritic nuclei textures as it grows from the isotropic phase [5]; the dendritic nuclei texture of the B_1 phase in compound **Ia** at 157°C (cooling) is shown in figure 2(*a*). As the temperature was further lowered, the dendritic nuclei rapidly coalesced into a structured mosaic-like texture [20]. After further cooling of compound **IIIa**, a typical mosaic-like texture of the B_1 phase was seen at 150°C, as shown in figure 2(*b*). Similar textural features of the B_1 phase were observed in compounds **IIa** and **IIb**. The transition enthalpies of the B_1–isotropic transition are in the range 12.6–14.9 kJ mol^{-1}.

For analogous compounds with the medium chain length (n=12) the B_2 phase was dominant, except that a monotropic B_1 phase was observed in compound **IIb** (X=F and Y=–COO–) due to the lateral fluorine. Hence, based on the same length of flexible chain (n=12), the B_2 phase is not favoured by the lateral *meta*-fluoro substitution of compound **IIb** compared with

Table 1. The transition temperatures (°C) and enthalpies (in parentheses, kJ mol^{-1})[a] of all compounds in series **I–III.**

Compound	Phase behaviour
Ia	Cr $\underset{103.8\ (-29.3)}{\overset{137.1\ (34.2)}{\rightleftharpoons}}$ B_1 $\underset{158.7\ (-14.9)}{\overset{160.8\ (15.1)}{\rightleftharpoons}}$ I
Ib	Cr $\underset{101.3\ (-20.6)}{\overset{91.3\ (-7.9)}{\rightleftharpoons}}$ Cr_1 $\underset{142.2\ (-18.2)}{\overset{132.4\ (32.1)}{\rightleftharpoons}}$ B_2 $\underset{}{\overset{145.3\ (18.5)}{\rightleftharpoons}}$ I
Ic	Cr $\underset{72.6\ (-6.5)}{\overset{102.4\ (67.3)}{\rightleftharpoons}}$ Cr_1 $\underset{138.4\ (-24.1)}{\overset{140.8\ (24.4)}{\rightleftharpoons}}$ B_2 $\underset{}{\overset{}{\rightleftharpoons}}$ I
IIa	Cr $\underset{112.6\ (-17.4)}{\overset{138.7\ (22.3)}{\rightleftharpoons}}$ B_1 $\underset{140.7\ (-14.0)}{\overset{142.7\ (14.5)}{\rightleftharpoons}}$ I
IIb	Cr $\underset{107.9\ (-24.8)}{\overset{129.0\ (48.4)}{\rightleftharpoons}}$ B_1 $\underset{117.3\ (-14.6)}{\overset{}{\rightleftharpoons}}$ I
IIc	Cr $\underset{96.7\ (-69.8)}{\overset{118.4\ (92.1)}{\rightleftharpoons}}$ B_2 $\underset{110.3\ (-20.8)}{\overset{}{\rightleftharpoons}}$ I
IIIa	Cr $\underset{131.3\ (-5.4)}{\overset{152.8\ (12.4)}{\rightleftharpoons}}$ Cr_1 $\underset{133.1\ (-16.3)}{\overset{155.2\ (6.0)}{\rightleftharpoons}}$ Cr_2 $\underset{160.0\ (-12.6)}{\overset{161.9\ (10.5)}{\rightleftharpoons}}$ B_1 $\underset{}{\overset{166.3\ (8.3)}{\rightleftharpoons}}$ Cr_3 I
IIIb	Cr $\underset{109.8\ (-16.7)}{\overset{116.3\ (-18.5)}{\rightleftharpoons}}$ Cr_1 $\underset{144.6\ (-13.3)}{\overset{160.4\ (59.8)}{\rightleftharpoons}}$ B_2 I
IIIc	Cr $\underset{104.0\ (-31.1)}{\overset{140.2\ (35.2)}{\rightleftharpoons}}$ B_2 $\underset{141.0\ (-18.7)}{\overset{143.4\ (18.6)}{\rightleftharpoons}}$ I

[a] Temperatures and enthalpies of transitions were determined by differential scanning calorimetry under N_2, heating and cooling at 5°C min^{-1}.

series **Ib** (X=H and Y=–COO–). An oval nuclei texture of the B_2 phase cooling from the isotropic liquid is observed to coalesce gradually to form a non-uniform texture. Compound **Ic** reveals schlieren and non-specific grainy texture regions at 128°C as shown in figure 3 (*a*), and compound **IIIb** displays spherulite domains and stripe textures coexisting with schlieren textures in some parts of small regions at 138°C, figure 3 (*b*), which demonstrate the characteristics of typical texture features observed in the B_2 phase [21–23]. Similar textural features of the B_2 phase were also observed in compounds **Ib**, **IIc** and **IIIc**. The transition enthalpies of the B_2–isotropic transition are in the range 13.3–24.1 kJ mol^{-1}.

(*a*)

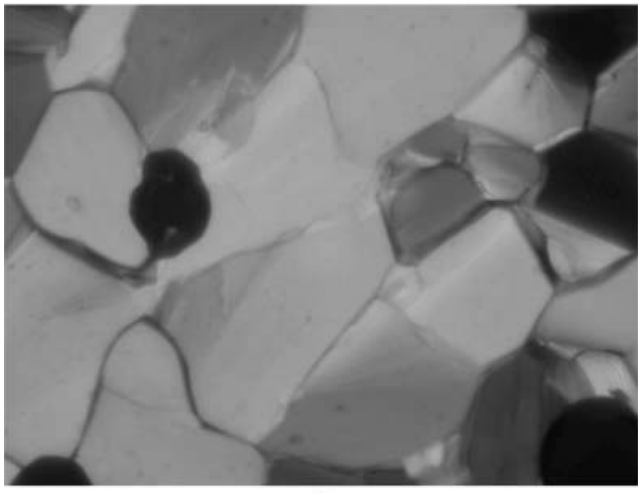

(*b*)

Figure 2. Polarizing optical micrographs of the B_1 phase obtained on cooling from the isotropic phase: (*a*) growth of dendritic nuclei of compound **Ia** at 157°C, (*b*) mosaic-like texture of compound **IIIa** at 150°C.

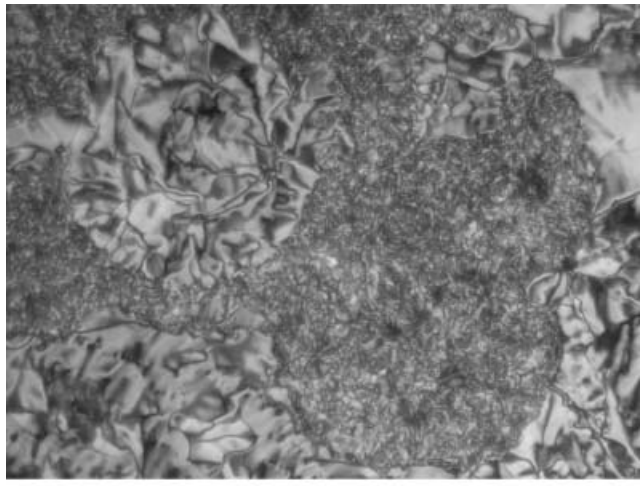

(*a*)

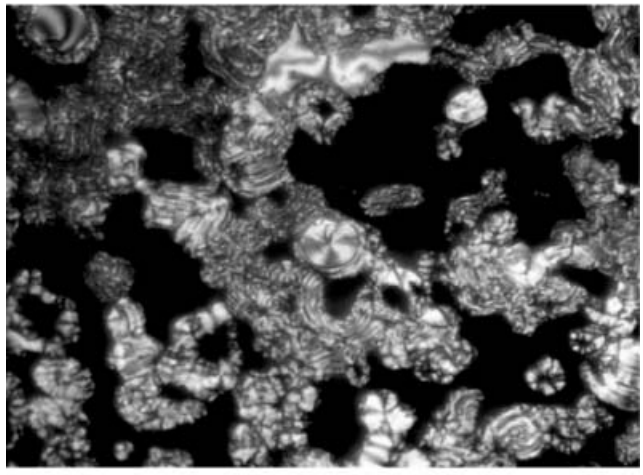

(*b*)

Figure 3. Polarizing optical micrographs of the B_2 phase obtained on cooling from the isotropic phase: (*a*) schlieren and non-specific grainy texture of compound **Ic** at 128°C, (*b*) spherulite domains and stripe textures of compound **IIIb** at 138°C.

Comparing analogous compounds among these three series, the lateral *meta*-fluoro-substituted derivatives of series **II** have the lowest isotropization temperatures and the Schiff base linkage derivatives of series **III** have the highest isotropization temperatures. Moreover, the lateral *meta*-fluoro-substituted derivatives of series **II** possess the narrowest mesophasic ranges of the B_1 and B_2 phases. This suggests that the dipolar effects and steric factors of lateral fluorine are detrimental to the formation of the B_1 and B_2 phases, especially the B_2 phase. Although the B_2 phase can be obtained by increasing the flexible chain length to $n=16$ in series **II**, compound **IIc** only displays a short range of a monotropic B_2 phase. Thereby, in contrast to the non-substituted series **I**, the lateral *meta*-fluoro substitution in series **II** destabilizes the B_2 phase.

3.2. *X-ray investigation*

In order to determine the structure of the mesophases by X-Ray diffraction (XRD), measurements were carried out in the mesophase temperature ranges of the compounds **Ic**, **IIa** and **IIIc** (non-oriented samples). The XRD pattern of the mesophase obtained from compound **IIa** at 125°C is shown in figure 4 (*a*). In the small angle region, two sharp reflection peaks are obtained at $d_1=26.2$ Å and $d_2=22.7$ Å; these reflections can be indexed as (1 1) and (0 2), respectively, for a

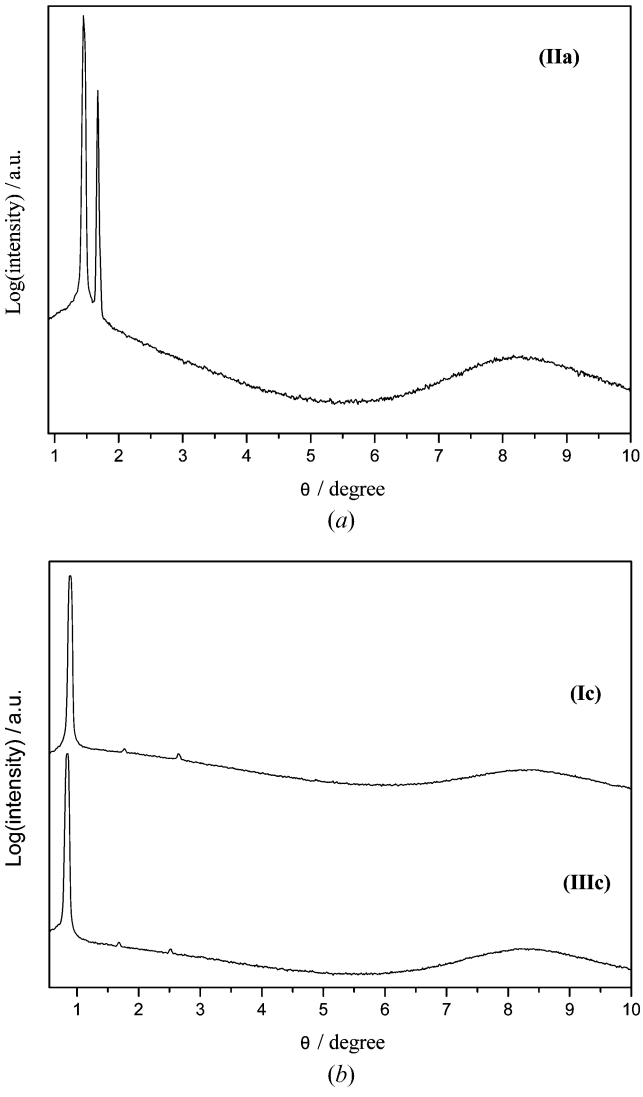

Figure 4. X-ray diffraction intensity against angle profiles obtained upon cooling from the isotropic phase: (*a*) in the B_1 phase of compound **IIa** at 125°C; (*b*) in the B_2 phase of compound **Ic** at 122°C and compound **IIIc** at 120°C (top and bottom, respectively).

centre-rectangular lattice with two-dimensional lattice parameters calculated as a=32.1 Å and b=45.4 Å, which can be identified as a B_1 phase (rectangular columnar mesophase, Col_r) as described in the literature [20, 24]. The molecular length (L) values of the banana-shaped molecular structures can be calculated by molecular modelling, on the assumtion that all molecular structures are coplanar, the bent rigid cores have a central bending angle of 120° [20, 25] and the alkyl chains are in the fully extended all-*trans* conformation. The value of the lattice parameter b corresponds approximately to the fully extended molecular length of 46.2 Å by molecular modelling calculation.

The XRD patterns of the mesophases obtained from compounds **Ic** and **IIIc** at 122 and 120°C, respectively, are shown in figure 4 (*b*). Compound **Ic** in the mesophase showed three sharp reflection peaks at d_1=42.9 Å, d_2=21.5 Å and d_3=14.4 Å, which can be indexed as (0 1), (0 2), and (0 3), in the small angle region. The layer (d) spacing values are in the ratio of 1 : 1/2 : 1/3, indicating that a lamellar order exists in the mesophase. Similar diffraction patterns for **IIIc** in the small angle region, viz. three sharp reflection peaks at d_1=45.5 Å, d_2=22.6 Å, and d_3=15.1 Å, again indicate lamellar order. This is clearly indicative of a two-dimensional structure of the B_2 phase, which has been confirmed in previous reports [26]. The d values determined from the XRD measurements are smaller than the calculated molecular length (L) values from molecular modelling, i.e. L=58.2 and 59.2 Å for compounds **Ic** and **IIIc**, respectively, indicating tilted smectic phases. From the values of d spacing (XRD) and L (molecular modelling), the tilt angle (α) can be calculated to be around 42.5° and 39.8° for compounds **Ic** and **IIIc**, respectively. In addition, wide angle diffuse peaks corresponding to a spacing value of 4.6 Å in figures 4 (*a*) and 4 (*b*) indicate that similar liquid-like in-plane orders with average intermolecular distances around 4.6 Å are prevalent inside the smectic layers of compounds **Ic**, **IIc** and **IIIc**.

3.3. *Electro-optical behaviour*

Spontaneous polarization ($\mathbf{P}_s$) experiments were carried out on LC cells of 9 μm thickness (antiparallel rubbing direction) by the triangular wave voltage method [27], the current response being measured across a 1 kΩ resistance. Regarding the electro-optical measurements, the most interesting compounds are **Ib**, **Ic**, **IIIb** and **IIIc**, because they exhibit the best mesomorphic properties and switching behaviour (i.e. B_2 phase). Since both B_{1rev} and $B_{1rev,tilt}$ phases exhibit switching phenomena on applying electric fields [14, 28], the B_1 phase is further confirmed by the electro-optical observation that the B_1 phase exhibits no switching phenomena or texture variation under polarizing microscopy, on applying an electric field. For instance, the spontaneous polarization of compounds **Ib** and **IIIb** were measured representatively (because both compounds exhibit the B_2 phase). The samples were slowly cooled ($1^\circ C\,min^{-1}$) from the isotropic phase to the mesophase under a triangular wave voltage. If a lower triangular wave voltage ($E\sim 2\,V\,\mu m^{-1}$) was applied, only one sharp peak was obtained in the $\mathbf{P}_s$ experiments. However, when a sufficiently higher triangular voltage ($E\sim 7\,V\,\mu m^{-1}$) was applied, a second peak became clearly visible and sharper. Thereafter, the current response peak became saturated above certain critical values of external fields.

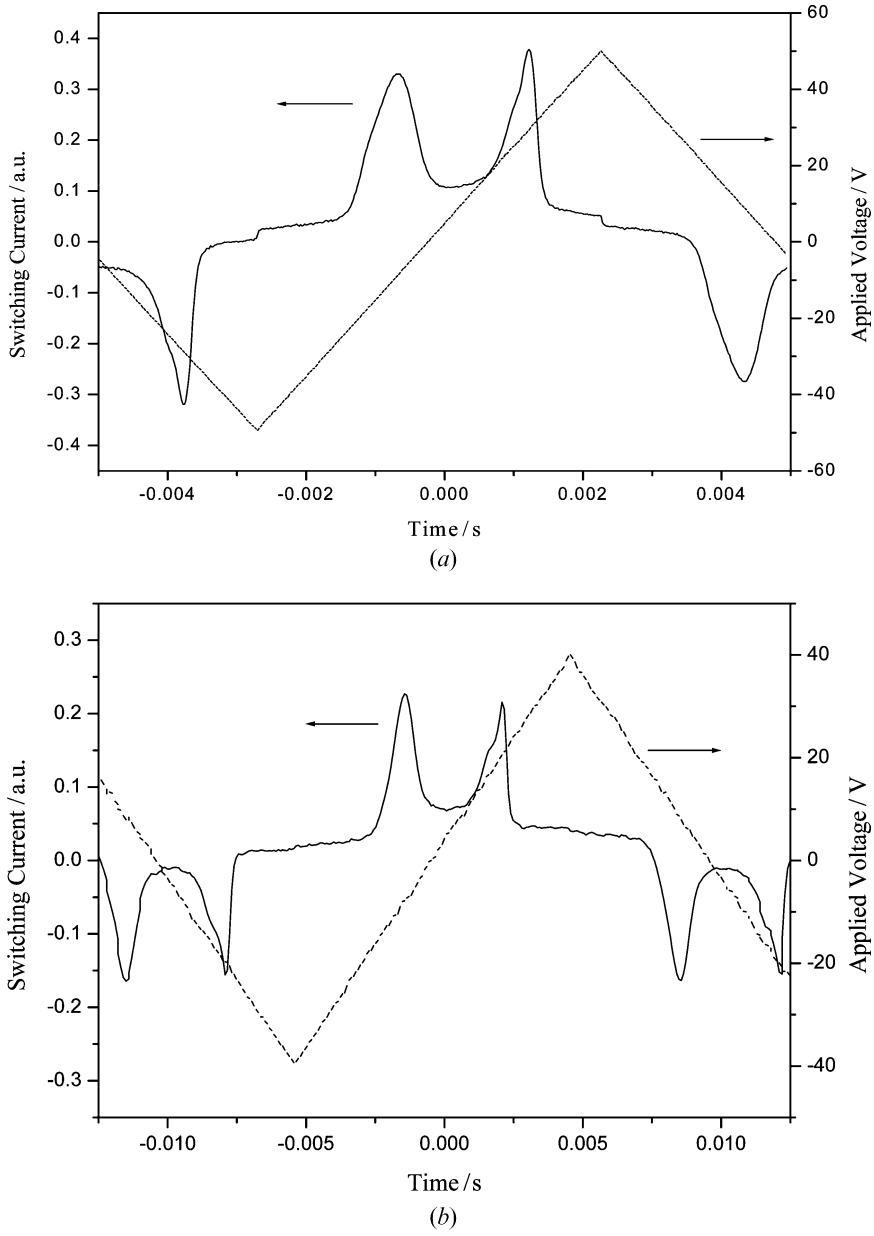

Figure 5. Switching current response on applying the triangular wave method (antiparallel rubbed 9 μm thick LC cells): (*a*) the B_2 phase of compound **Ib** at 132°C (V_{pp}=100 V, f=100 Hz); (*b*) the B_2 phase of compound **IIIb** at 134°C (V_{pp}=80 V, f=50 Hz).

Two current peaks per half-period of an applied triangular voltage are obtained in the switching current response curve of compounds **Ib** and **IIIb**, as shown in figures 5 (*a*) and 5 (*b*), respectively. The two-peak response is the characteristic behaviour of a sequential electric response due to a ferroelectric state switched into an antiferroelectric ground state and back to the opposite ferroelectric state; so this result confirms the $SmCP_A$ structure of the B_2 phase in compounds **Ib** and **IIIb** [29]. The $\mathbf{P}_s$ values calculated by integrating the area under the switching current peaks are estimated to be *c*. 940 nC cm^{-2} for compound **Ib** at 132°C, and 820 nC cm^{-2} for compound **IIIb** at 134°C.

Figure 6 shows the values of spontaneous polarization plotted as a function of the temperature for compounds **Ic** and **IIIc**. On cooling from the isotropic phase, the spontaneous polarizations increase initially with decreasing temperature, then level off. The abrupt increase of $\mathbf{P}_s$ around the isotropization temperature indicates that the I-B_2 phase transition is of first order. The $\mathbf{P}_s$ value exhibits maxima of 895 nC cm^{-2} for compound **Ic** at 127°C and 680 nC cm^{-2} for **IIIc** at

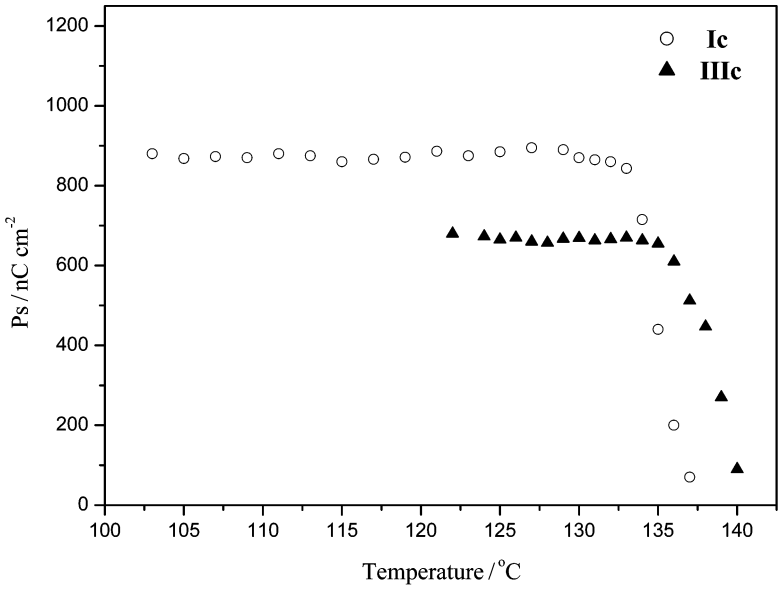

Figure 6. Temperature dependence of spontaneous polarization in the B_2 phase of compounds **Ic** and **IIIc** (antiparallel rubbed 9 μm thick LC cells).

122°C. The $\mathbf{P}_s$ measurements for compound **IIc** are not shown in figure 6 because of its narrow mesophase range; its maximum $\mathbf{P}_s$ value is about 368 nC cm^{-2} at 104°C. In comparison, the $\mathbf{P}_s$ value of compound **IIc** (368 nC cm^{-2}) is much smaller than that of the analogous compound **Ic** (895 nC cm^{-2}) without the lateral *meta*-fluoro-substitution.

Figures 5 and 6 suggest that the $\mathbf{P}_s$ values of compounds **Ib** and **Ic** (940 nC cm^{-2} and 895 nC cm^{-2}, respectively) are larger than those of the analogous compounds **IIIb** and **IIIc** (820 nC cm^{-2} and 680 nC cm^{-2}, respectively), by reason of the different linking groups (on the side wings) in series **I** (Y= –COO–) and series **III** (Y=–CH=N–). In addition, compounds **Ib** and **IIIb** have larger $\mathbf{P}_s$ values than the respective compounds **Ic** and **IIIc** owing to different lengths of the flexible terminal chains. Thus, the order of $\mathbf{P}_s$ values in relation to molecular design is as follows: $\mathbf{P}_s$ (without fluoro-substitution)>$\mathbf{P}_s$ (with lateral *meta*-fluoro-substitution on the middle outer rings); $\mathbf{P}_s$ (*Y*= –COO–, linking group on the side wings)>$\mathbf{P}_s$ (*Y*= –CH=N–); $\mathbf{P}_s$ (*n*=12, shorter flexible chains)>$\mathbf{P}_s$ (*n*=16, longer flexible chains).

In order to investigate the dynamics of the polarization switching behaviour, the switching currents of compound **Ib** in 9 μm thick LC cells (antiparallel rubbed) were measured with an applied square wave field (V_{pp}=80 V, *f*=10 Hz) in the B_2 phase, at 121°C on cooling from the isotropic phase. The resulting switching current curves are shown in figure 7 (*a*) as a function of time. The switching time (τ) values were determined from the time elapsed between the appearance of the maximum of the current signal and the field reversal [30]. The switching time as a function of temperature is shown in figure 7 (*b*) with the same field and frequency. A decrease in the switching time with increasing temperature for both compounds **Ib** and **IIIc** (in the range 10–40 μs) was observed. The switching time of compound **Ib** (*n*=12, *Y*=–COO–, $\mathbf{P}_s$=940 nC cm^{-2}) is a little larger than that of compound **IIIc** (*n*=16, *Y*= –CH=N–, $\mathbf{P}_s$=680 nC cm^{-2}), with less difference at higher temperatures. The switching time is influenced by viscosity but is unrelated to the $\mathbf{P}_s$ value.

On slow cooling of compound **Ib** from the isotropic phase, the mesophase gradually appeared and coalesced as small fractal domains; non-specific grainy domains along with small fan-like domains developed at 125°C on further cooling. By applying a sufficiently high electric field (**E**~7 V μm^{-1}), the texture was transformed into a fan-like texture. As the electric field was removed, the switched off state relaxed back to a state with non-specific texture, possessing only very small irregularly distributed bright spots, which was nearly dark between crossed polarizers, see figure 8 (*a*). When one polarizer was rotated clockwise by a small angle (*c*. 10°) from the crossed position, dark and bright domains become clearly distinguishable. On rotating the polarizer counterclockwise by the same angle from the crossed position, the previously dark domains became bright and *vice versa*, see figures 8 (*b*) and 8 (*c*). This observation is indicative of the occurrence of chiral domains with opposite handednesses. Thus, two types of

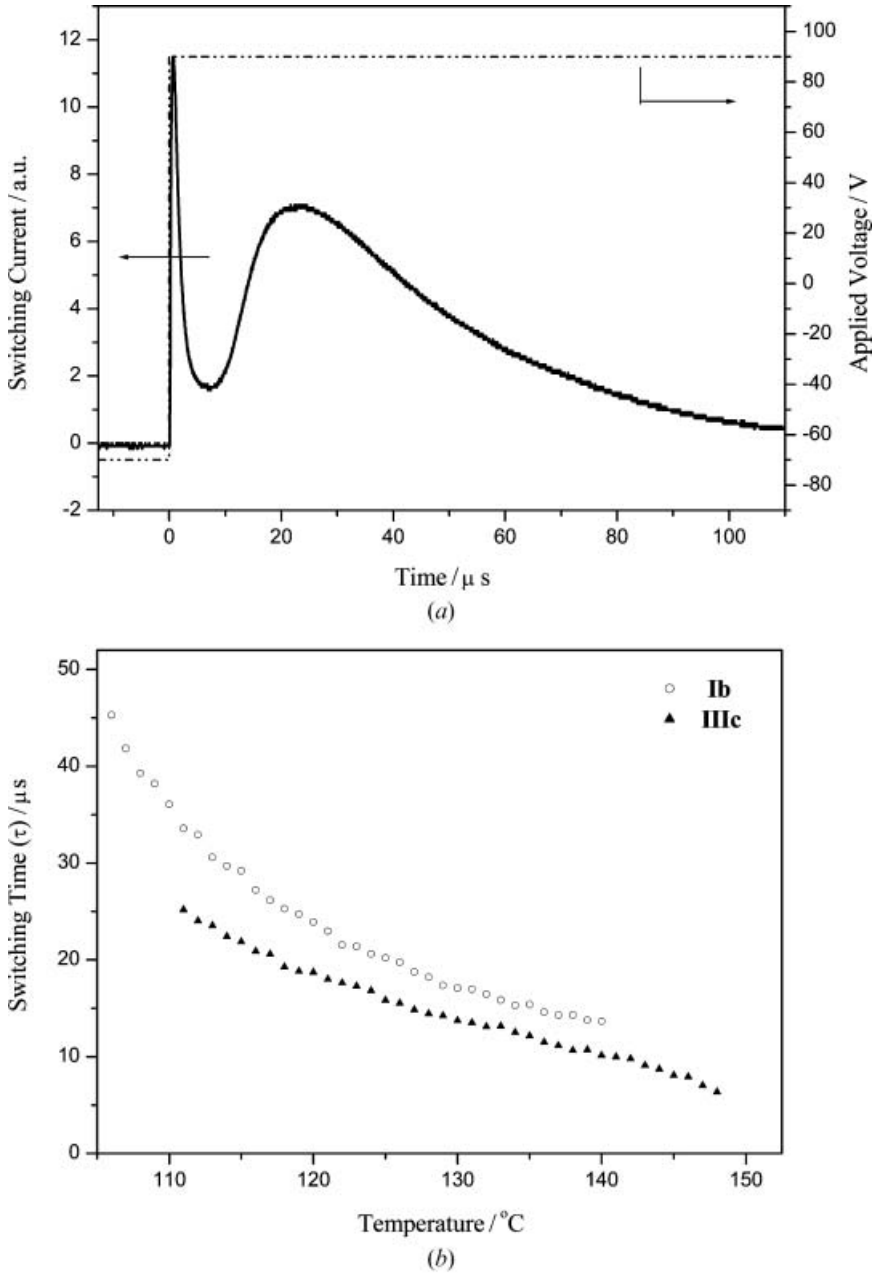

Figure 7. (*a*) Time dependences of the switching current under a square wave field for compound **Ib** at 121°C; (*b*) switching time as a function of temperature for compounds **Ib** and **IIIc** (antiparallel rubbed 9 μm thick LC cells, $V_{pp}=80$ V, $f=10$ Hz).

optically active domain with opposite chiralities were formed; this phenomenon of exchanging brightness with rotation of the polarizer against the analyser, counter-clockwise or clockwise, has been reported previously [13].

In order to investigate further the switching process of the B_2 phase, a d.c. electric field was applied to antiparallel rubbed 9 μm thick LC cells between crossed polarizers [29]. When the isotropic phase was slowly cooled (0.5°C min^{-1}) in the presence of a high d.c. field (about 60 V), large and intact circular domains were induced. Moreover, many circular domains were formed in the B_2 phase in which the smectic layers were circularly arranged around the centres of the domains. The layer structure arrangement corresponds to the domain models proposed by Link *et al*. [7]. After removing the electric fields, the extinction crosses were reoriented along the crossed polarizer position in the off

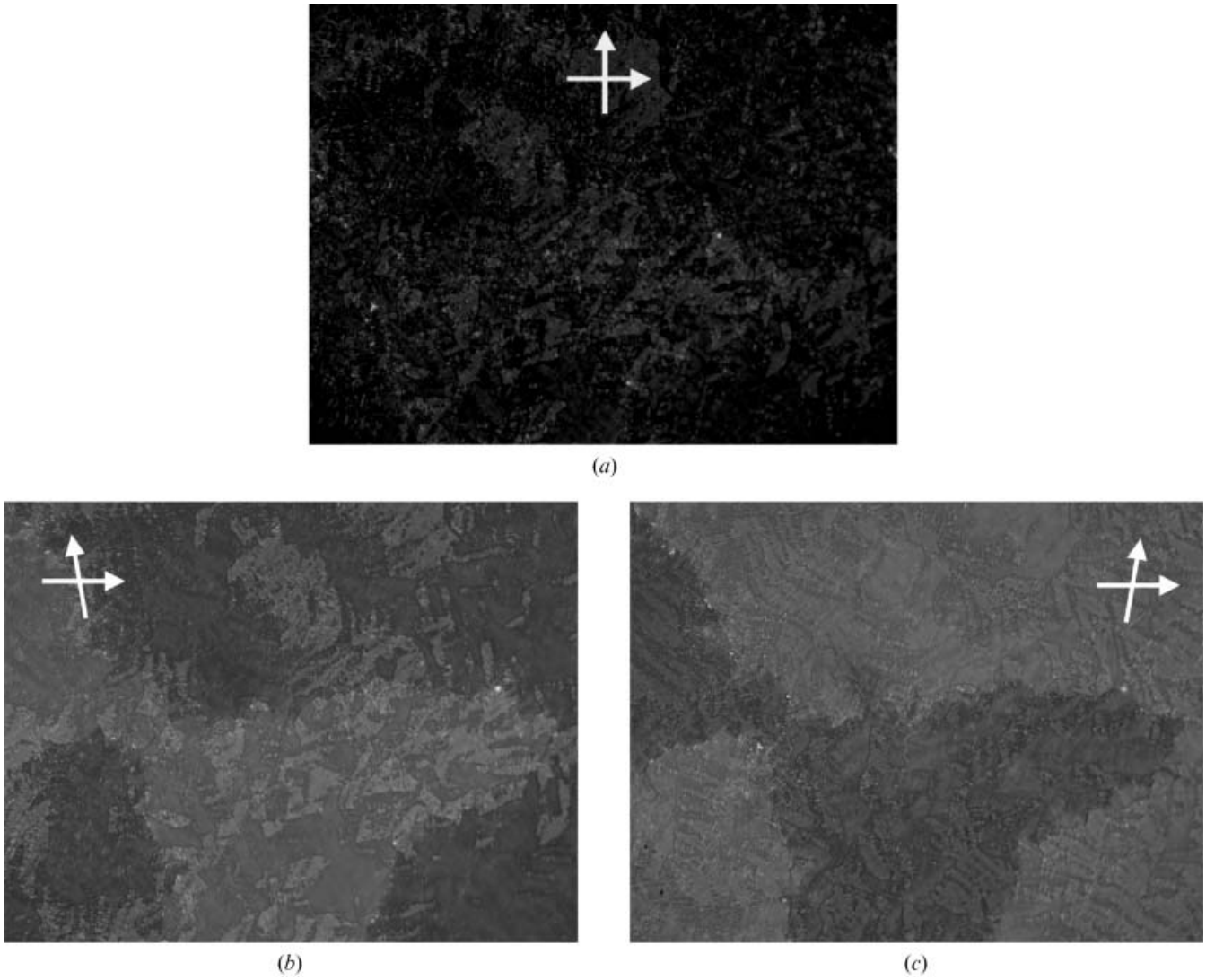

Figure 8. Polarizing optical microscopic texture of the B_2 phase in compound **Ib** after removing the electric field at 125°C (cooling): (*a*) crossed position, (*b*) and (*c*) rotation of the polarizer counterclockwise and clockwise, respectively, from the crossed polarizer position. (Arrows are the directions of polarizers and analysers.)

state, see figure 9 (*a*), indicating an anticlinic tilt in the antiferroelectric ground state (SmC_AP_A). As shown in figures 9 (*b*) and 9 (*c*), on applying electric fields with reverse polarities, the extinction crosses rotated counterclockwise (positive field) and clockwise (negative field). The extinction crosses in the switched on state did not coincide with the crossed polarizer positions in the off-state. The angles between the extinction directions and the crossed polarizer positions are about 41° for ± 60 V at 124°C, which corresponds to the optical tilt angle. The switching behaviour of the extinction crosses of domains rotated in opposite directions, depending on the sign of the field, is characteristic of field-responsive textures for chiral domains of the B_2 phase [31]. However, the extinction crosses should rotate in only one direction in the racemic domains, independent of the sign of the field, which is characteristic of field-responsive textures for racemic domains of the B_2 phase (see figure 10). The angles between the extinction directions and the crossed polarizer positions are about 37° for ± 60 V at 127°C [32].

The switching process can also be studied by measuring the tilt angle as a function of applied d.c. electric fields in the B_2 phase of compounds **Ic** and **IIIc** (at 124 and 130°C, respectively), as shown in figure 11. The tilt angles are estimated from the angles of rotation between the extinction brushes and crossed polarizers on applying an electric field, which indicates that a rotated phase structure from the anticlinic-antiferroelectric (SmC_AP_A) state to the synclinic-ferrelectric

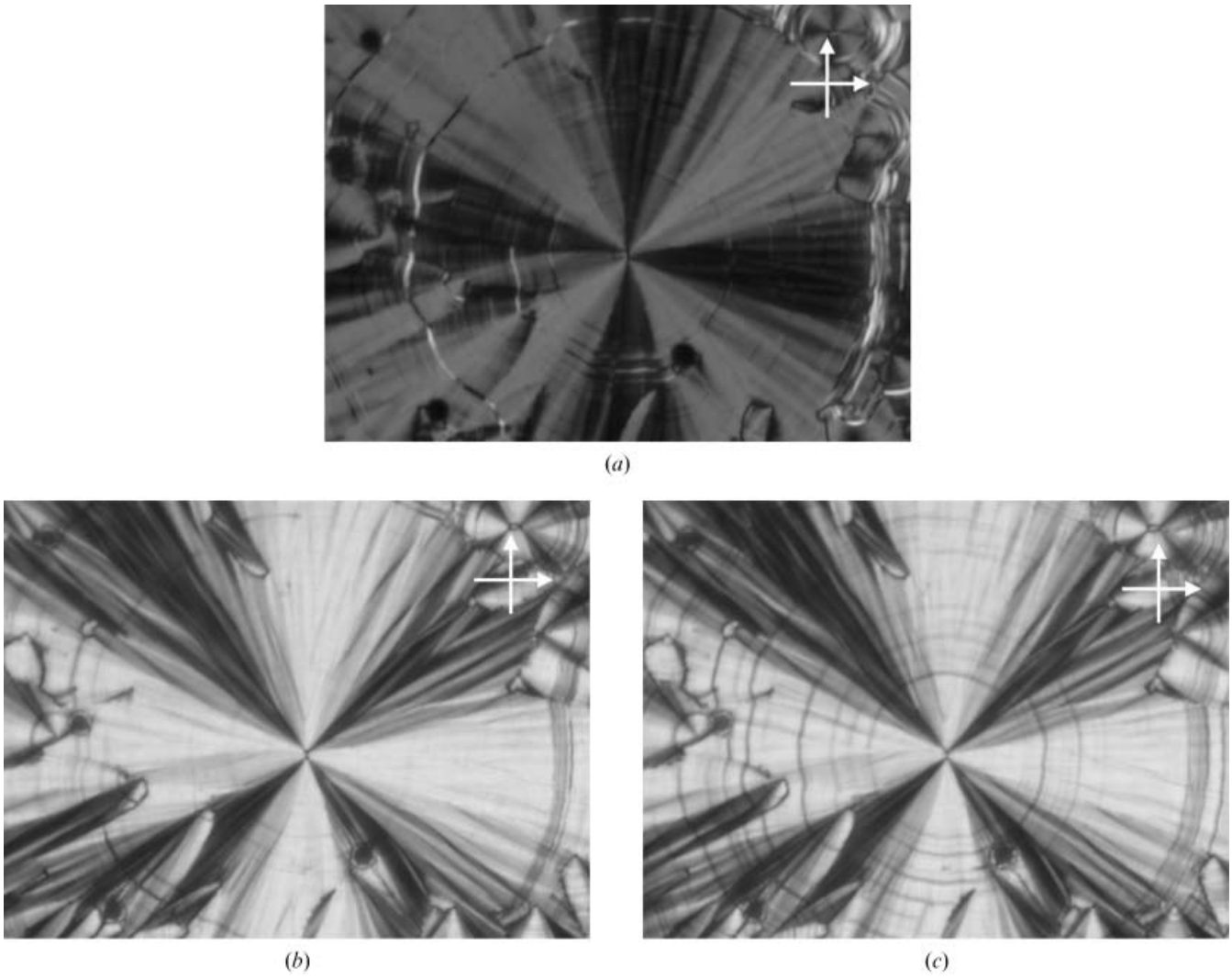

Figure 9. Polarizing optical micrographs of the circular domains in the B_2 phase for compound **Ic** (antiparallel rubbed 9 µm thick LC cells). Chiral domains obtained by various d.c. fields: (*a*) 0 V, SmC_AP_A, (*b*) −60 V, SmC_SP_F, (*c*) +60 V, SmC_SP_F at 124°C. (Arrows are the directions of polarizers and analysers.)

(SmC_SP_F) state has occurred. The tilt angles of both compounds increase with increasing applied voltage, and saturate at fields of 28 V and 17 V for compounds **Ic** and **IIIc**, respectively. Moreover, both compounds **Ic** and **IIIc** have similar tilt angles at lower applied voltages and similar saturated tilt angles around 40°.

Optical transmission studies were carried out on the B_2 phase of compound **Ic** in 6 µm thick LC cells (antiparallel rubbed) using a triangular wave voltage (V_{pp}=60 V, f=1 Hz) at 129°C. The electric field dependence of the transmitted light intensity is shown in figure 12. The switching process exhibits a thresholdless V-shaped behaviour, with highest transmittance at around 30 V; a similar phenomenon has been observed in another bent-core structure [33]. This result should coincide with the previous title angle experiment of compound **Ic**, where the highest transmittance at around 30 V is due to the saturated title angle at around 28 V (see figure 11); the turn on voltage is below 2 V. The V-shaped or pseudo-V-shaped electro-optical response in transmittance is abruptly increased on increasing the applied voltage from below 7 V, then is gradually relaxed near saturation at around 30 V. The shape of the electro-optical response curve and turn on voltage in transmittance may be further improved by reducing the thickness of the LC cell.

4. Conclusions

Three analogous series of achiral banana-shaped liquid crystalline molecules containing bisnaphthyl units and

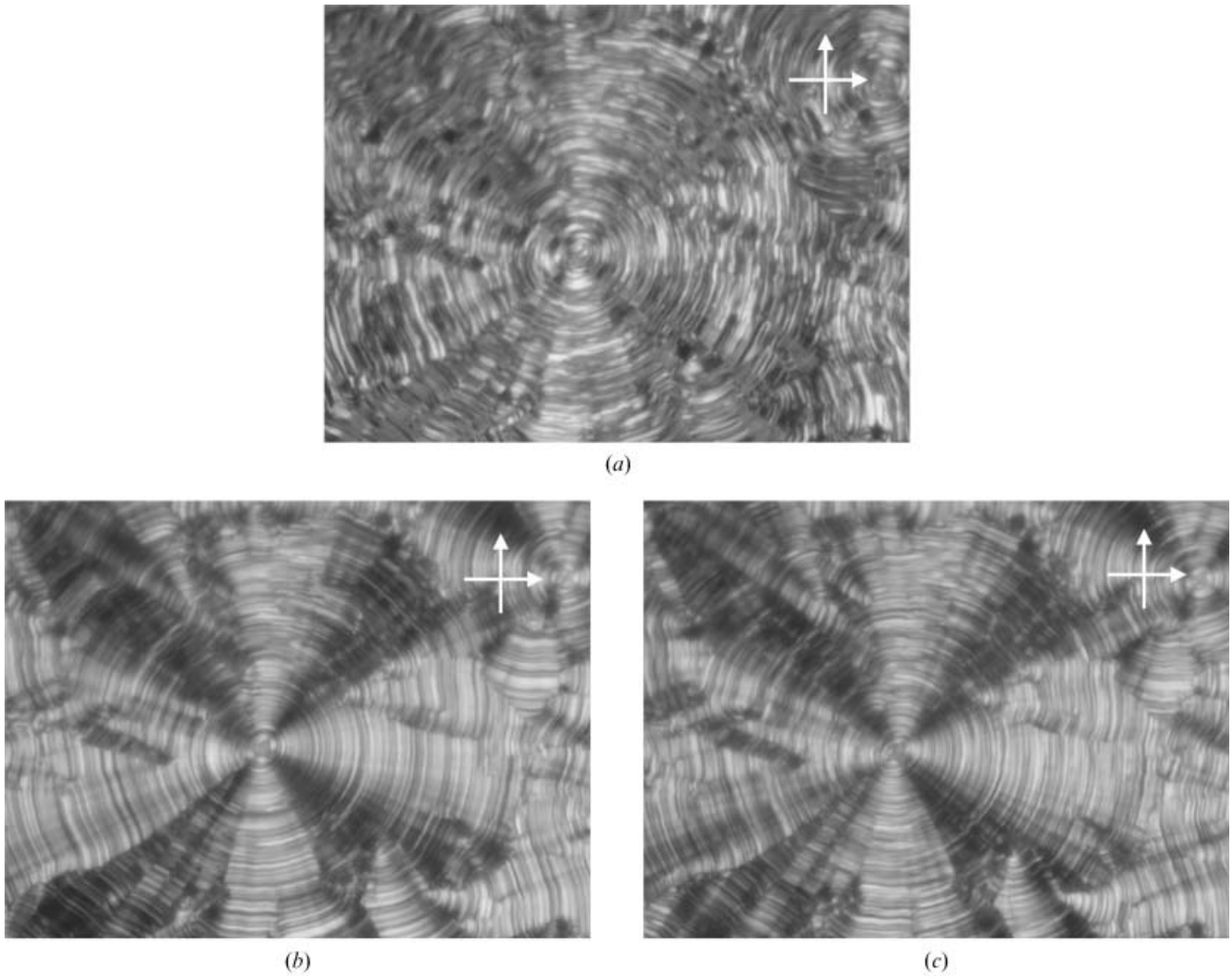

Figure 10. Polarizing optical micrographs of the circular domains in the B_2 phase for compound **Ic** (antiparallel rubbed 9 μm thick LC cells). Racemic domains obtained by various d.c. fields: (*a*) 0 V, SmC_SP_A, (*b*) −60 V, SmC_AP_F, (*c*) +60 V, SmC_AP_F at 127°C. (Arrows are the directions of polarizers and analysers.)

derived from resorcinol cores have been prepared. The formation of the B_2 phase with antiferroelectric switching behaviour is favoured in the achiral bisnaphthyl derivatives with longer flexible chains; however, the B_1 phase is favoured in corresponding derivatives with shorter flexible chains. The B_1 and B_2 phases are less favoured in compounds of series **II** with lateral *meta*-fluoro-substitution on the middle outer phenyl rings, in comparison with series **I** without fluoro-substitution. The B_1 or B_2 phases have been confirmed by XRD and POM measurements. The electro-optical switching behaviour of two current peaks found during a triangular voltage half-period has also confirmed the B_2 phase. This process exhibits an electric field-induced transition from an antiferroelectric (tristable) state to a ferroelectric (bistable) state. The spontaneous polarization (by switching current response), tilt angle of chiral domains (by POM), and transmittance–voltage measurements of the B_2 phase in related compounds have been surveyed in this study.

Acknowledgements

The powder XRD measurements were supplied by beamline BL17A (operated by Dr J.-J. Lee) of the National Synchrotron Radiation Research Center (NSRRC), Taiwan. Financial support provided by the National Science Council of Taiwan, ROC through NSC 92-2113-M-009-016, and AUO (Taiwan) through NCTU-94C060 is acknowledged.

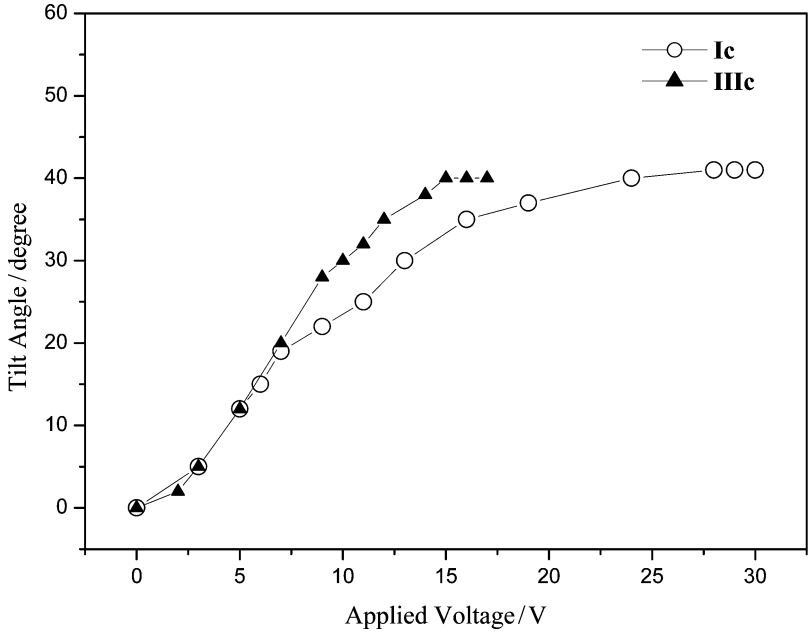

Figure 11. Tilt angle of the B_2 phase as a function of d.c. electric field in compounds **Ic** and **IIIc** (antiparallel rubbed 9 μm thick LC cells) at 124 and 130°C, respectively.

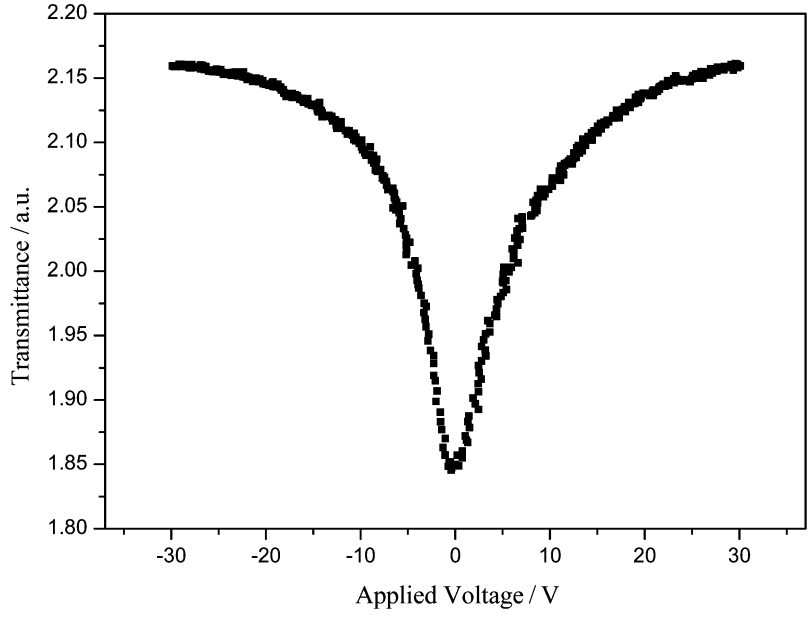

Figure 12. Transmittance versus applied voltage (triangular wave, V_{pp}=60 V, f=1 Hz) in the B_2 phase of compound **Ic** (antiparallel rubbed 6 μm thick LC cells) at 129°C.

References

[1] R.B. Meyer, L. Liebert, L. Strzelecki, P. Keller. *J. Phys. (Paris) Lett.*, **36**, L69 (1975).
[2] A.D.L. Chandani, Y. Ouchi, H. Takezoe, A. Fukuda, K. Terashima, K. Furukawa, A. Kishi. *Jpn. J. appl. Phys.*, **28**, L1261 (1989).
[3] A. Fukuda, Y. Takanishi, T. Isokaki, K. Ishikawa, H. Takezoe. *J. mater. Chem.*, **4**, 997 (1994).
[4] T. Niori, T. Sekine, J. Watanabe, T. Furukawa, H. Takezoe. *J. mater. Chem.*, **6**, 1231 (1996).
[5] G. Pelzl, S. Diele, W. Weissflog. *Adv. Mater.*, **11**, 707 (1999).
[6] J.P. Bedel, J.C. Rouillon, J.P. Marcerou, M. Laguerre, H.T. Nguyen, M.F. Achard. *Liq. Cryst.*, **28**, 1285 (2001).

[7] D.R. Link, G. Natale, R. Shao, J.E. Maclennan, N.A. Clark, E. Körblova, D.M. Walba. *Science*, **278**, 1924 (1997).
[8] W. Weissflog, H. Nàdasi, U. Dunemann, G. Pelzl, S. Diele, A. Eremin, H. Kresse. *J. mater. Chem.*, **11**, 2748 (2001).
[9] M.W. Schröder, S. Diele, G. Pelzl, U. Dunemann, H. Kresse, W. Weissflog. *J. mater. Chem.*, **13**, 1877 (2003).
[10] R.A. Reddy, B.K. Sadashiva, V.A. Raghunathan. *Chem. Mater.*, **16**, 4050 (2004).
[11] C. Keith, R.A. Reddy, C. Tschierske. *Chem. Commun.*, **7**, 871 (2005).
[12] C. Achten, R. Cuypers, M. Giesbers, A. Koundijs, A.T.M. Marcelis, E.J.R. Sudhölter. *Liq. Cryst.*, **31**, 1167 (2004).
[13] M.W. Schröder, S. Diele, G. Pelzl, W. Weissflog. *ChemPhysChem*, **5**, 99 (2004).
[14] D. Kardas, M. Prehm, U. Baumeister, D. Pociecha, R.A. Reddy, G.H. Mehl, C. Tschierske. *J. mater. Chem.*, **15**, 1722 (2005).
[15] R. Güller, A. Binggeli, V. Breu, D. Bur, W. Fischi, G. Hirth, C. Jenny, M. Kansy, F. Montavon, M. Müller, C. Oefner, H. Vieira, M. Wilhelm, W. Wostl, H.P. Mätki. *Bioorg. med. Chem. Lett.*, **9**, 1403 (1999).
[16] M. Debono, W.W. Turner, L. LaGrandeur, F.J. Burkhadt, J.S. Nissen., et al. *J. med. Chem.*, **38**, 3271 (1995).
[17] R. Gomez, J.L. Segura, N. Martin. *J. org. Chem.*, **65**, 7501 (2000).
[18] C. Cativiela, J.L. Serrano, M.M. Zurbano. *J. org. Chem.*, **60**, 3074 (1995).
[19] A. Svensson, T. Fex, J. Kihlberg. *Tetrahedron Lett.*, **37**, 7649 (1996).
[20] D. Shen, S. Diele, G. Pelzl, I. With, C. Tschierske. *J. mater. Chem.*, **9**, 661 (1999).
[21] T. Sekine, T. Niori, M. Sone, J. Watanabe, S.W. Choi, Y. Takanishi, H. Takezoe. *Jpn.J. appl. Phys.*, **36**, 6455 (1997).
[22] H. Dehne, M. Pötter, S. Sokolowski, W. Weissflog, S. Diele, G. Pelzl, I. Wirth, H. Kresse, H. Schmalfuss, S. Grande. *Liq. Cryst.*, **28**, 1269 (2001).
[23] R.A. Reddy, B.K. Sadashiva. *Liq. Cryst.*, **30**, 1031 (2003).
[24] G. Dantlgraber, D. Shen, S. Diele, C. Tschierske. *Chem. Mater.*, **14**, 1149 (2002).
[25] J. Ortega, M.R. de la Fuente, J. Etxebarria, C.L. Folcia, S. Díez, J.A. Gallastegui, N. Gimeno, M.B. Ros, M.A. Pérez-Jubindo. *Phys. Rev. E.*, **69**, 011703 (2004).
[26] V (*a*) Prasad, S.W. Kang, S. Kumar. *J. mater. Chem.* **13**, 1259 (2003); (*b*) H.N. Shreenivasa Murthy, B.K. Sadashiva. *Liq. Cryst*., **31**, 1337 (2004).
[27] K. Miyasato, S. Abe, H. Takezoe, A. Fukuda, E. Kuze. *Jpn. J. appl. Phys.*, **22**, L661 (1983).
[28] J. (*a*) Mieczkowski, K. Gomola, J. Koseska, D. Pociecha, J. Szydlowska, E. Gorecka. *J. mater. Chem.* **13**, 2132 (2003); (*b*) E. Gorecka, N. Vaupotič, D. Pociecha, M. Čepič, J. Mieczkowski. *ChemPhysChem*, **6**, 1087 (2005); (*c*) K. Pelz, W. Weissflog, U. Baumeister, S. Diele. *Liq. Cryst*., **30**, 1151 (2003).
[29] M. Zenyoji, Y. Takanishi, K. Ishikawa, J. Thisayukta, H. Watanabe, J. Takezoe. *J. mater. Chem.*, **9**, 2775 (1999).
[30] C.V. Yelamaggad, U.S. Hiremath, S. Anitha Nagamani, D.S. Shankar Rao, S. Krishna Prasad. *J. mater. Chem.*, **11**, 1818 (2001).
[31] D. Shen, A. Pegenau, S. Diele, I. Wirth, C. Tschierske. *J. Am. chem. Soc.*, **122**, 1593 (2000).
[32] S. Shubashree, B.K. Sadashiva, S. Dhara. *Liq. Cryst.*, **29**, 789 (2002).
[33] A. Jákli, Y.M. Huang, K. Fodor-Csorba, A. Vajda, G. Galli, S. Diele, G. Pelzl. *Adv. Mater.*, **15**, 1606 (2003).